View metadata, citation and similar papers at core.ac.uk

brought to you by CORE

provided by Boise State University - ScholarWorks

PARAMETER ESTIMATION AND DYNAMIC STATE OBSERVER DESIGN FOR VAPOR COMPRESSION SYSTEMS

by

Travis D. Pruitt

A thesis

submitted in partial fulfillment

of the requirements for the degree of

Master of Science in Mechanical Engineering

Boise State University

August 2019

© 2019

Travis D. Pruitt

ALL RIGHTS RESERVED

BOISE STATE UNIVERSITY GRADUATE COLLEGE

DEFENSE COMMITTEE AND FINAL READING APPROVALS

of the thesis submitted by

Travis D. Pruitt

Thesis Title: Parameter Estimation and Dynamic State Observer Design for Vapor Compression Systems

Date of Final Oral Examination: 7 June 2019

The following individuals read and discussed the thesis submitted by student Travis D. Pruitt, and they evaluated his presentation and response to questions during the final oral examination. They found that the student passed the final oral examination.

John F. Gardner, Ph.D.	Chair, Supervisory Committee
Donald Plumlee, Ph.D.	Member, Supervisory Committee
Ralph S. Budwig, Ph.D.	Member, Supervisory Committee

The final reading approval of the thesis was granted by John F. Gardner, Ph.D., Chair of the Supervisory Committee. The thesis was approved by the Graduate College.

ACKNOWLEDGEMENTS

I would like to take a moment to thank those who's mentorship and guidance has been greatly appreciated throughout, not only this thesis, but my academic career altogether. First, Dr. John Gardner. Not only has Dr. Gardner become a good friend, but the experience I've gained working with him on various projects over the past several years has been invaluable. Thank you for your continued support and patients while I finished this thesis while working full-time.

I would also like to thank Dr. Plumlee and Dr. Budwig for their insight and direction that helped me to bring this thesis to completion. I was fortunate enough to have had the opportunity to attend classes taught by each of you, and truly appreciate the impact each of you had on both my academic and professional careers.

Finally, I would like to thank my wife, as well as my family for their unconditional support no matter what challenges I take on.

ABSTRACT

Between cooling our house, our workplace, and keeping our food cold both in home and commercially (among other uses), the vapor compression cycle (VCC) is a common method for removing heat from various environments and it accounts for a significant amount of the energy used throughout the world. Therefore, with an ever-growing demand for more efficient processes and reduced energy consumption, improving the ability to accurately model, predict the performance of, and control VCC systems is beneficial to society as whole.

While there is much information available regarding the performance for some of the components found in VCC systems, much of the challenge associated with modelling the VCC lies within the complex behavior of the heat exchangers found within the system. Over the years, lumped parameter models have been developed for the VCC. However, many of these rely on simplified geometry (mainly a bare tube assumption), and neglect to capture the effect of the fins found throughout those heat exchangers.

This thesis builds upon approaches used in the past by identifying effective heat transfer coefficients that capture this effect. Using this approach, a 2-ton residential air-conditioning unit was modelled, which was able to predict the heat removed by the VCC system within ±4% error when compared to published performance data from the manufacturer. Furthermore, these coefficients, along with the complete dynamic model, form the basis of a nonlinear state observer which can be used to further the ability to accurately predict and monitor system performance.

TABLE OF CONTENTS

LIST OF TABLES

LIST OF FIGURES

CHAPTER ONE: INTRODUCTION

The vapor compression cycle (VCC) is the most common refrigeration cycle used to remove heat from a wide variety of processes. (Cengel & Boles, 2015) From large scale commercial cooling to single residence HVAC and refrigeration, the VCC accounts for a significant amount of the energy used throughout the world. However, even with its frequent use, the ability to monitor real time performance or apply advanced control algorithms in VCC systems is still very limited. With an ever-growing demand for more efficient processes and reduced energy consumption, improving our collective ability to model, predict the performance of, and control VCC systems could benefit society as a whole.

Although the VCC can be used for heating, this thesis will focus mainly on cooling, specifically its application in residential air conditioning. In this case, the major equipment utilized throughout the process includes; a compressor, two cross-flow heat exchangers (the evaporator and condenser), and flow restricting devices such as a fixed orifice, expansion valve, etc. A basic visual representation of this system can be seen below in Figure 1.

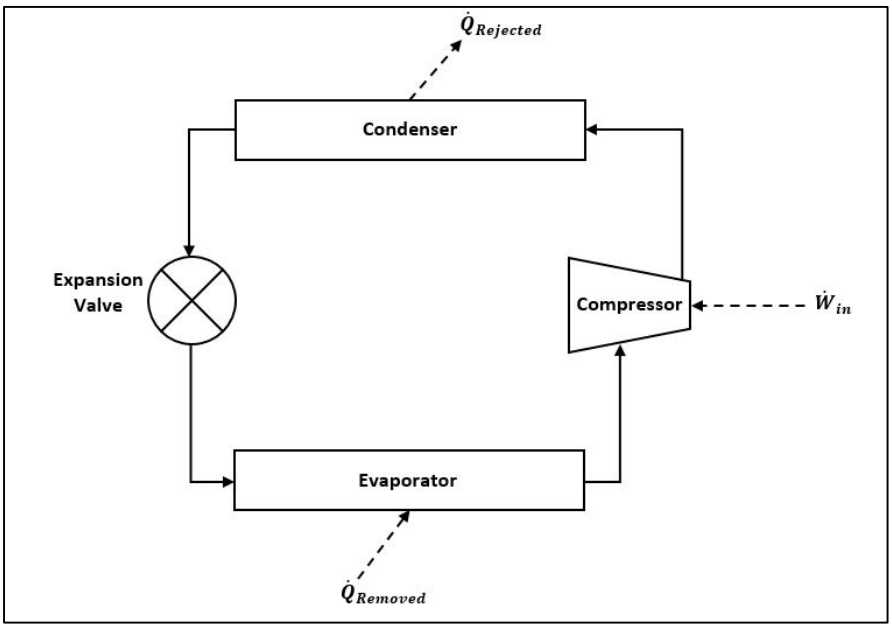

Figure 1. General VCC Schematic.

The system uses refrigerant to remove heat from a target space, then reject said heat to a separate area or atmosphere using those major components described above. While there is much information available regarding the performance of expansion valves and compressors, much of the challenge associated with modelling the VCC lies within the complex behavior of the heat exchangers. Both the evaporator and condenser are made up of extensive lengths of tubing surrounded by fins that augment the heat transfer into the former, and out of the latter (example of condenser tubing and fins shown in Figure 2).

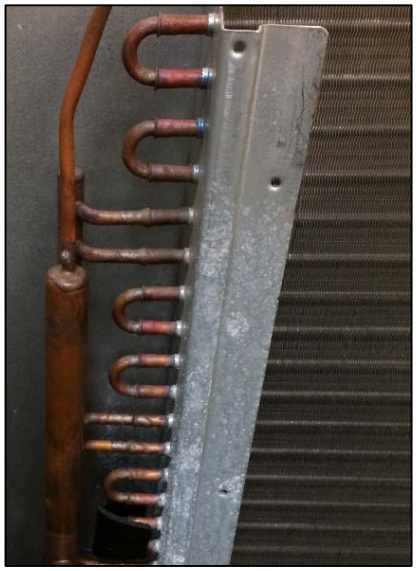

Figure 2. Condenser Tubing and Portion of Fins on Residential HVAC unit.

However, previous modelling attempts (discussed further below), frequently utilize equations describing a bare tube to estimate the heat transfer between the refrigerant and its surroundings. While this assumption simplifies the parameter identification, it doesn't accurately capture what is occurring and ignores a significant component of the system.

In addition, the refrigerant flowing through each heat exchanger experiences various phase changes depending on its thermodynamic state and location throughout the cycle. A summary of the thermodynamic states throughout the VCC can be outlined as shown in Table 1 (which refers to Figure 3) below:

Table 1. Thermodynamic States of a VCC System.

State	Refrigerant Phase
1	Superheated vapor at low side pressure at compressor inlet
2	Superheated vapor at high side pressure and elevated temperature at compressor outlet
2’	Saturated vapor at high side pressure
2’’	Saturated liquid at high side pressure
2’’’	Subcooled liquid at high side pressure at condenser outlet
3	Subcooled liquid at lower pressure and temperature at expansion valve
4	Saturated mixture at low side pressure at evaporator inlet
4’	Saturated vapor at low side pressure

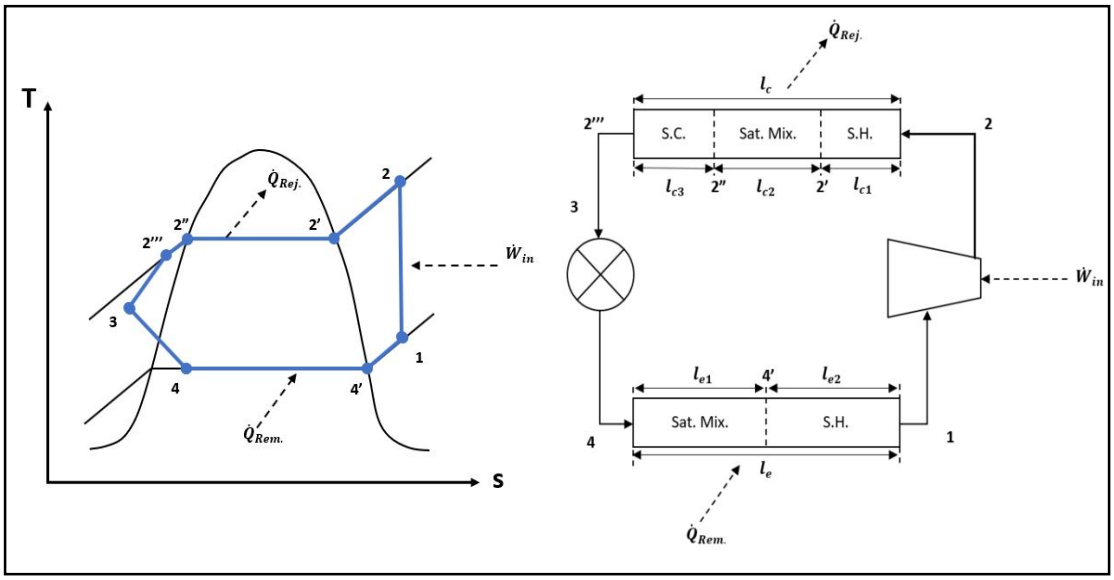

Figure 3. T-s diagram (left), system representation (right) for VCC system.

To model this cycle in such a way to be useful when either controlling or monitoring the system, it is important to consider the various modelling approaches that can be used, as well as the benefits associated with that method. For example, a lumped parameter system model is a common approach to simplifying the modelling process.

This approach breaks each heat exchanger into various segments or control volumes to be evaluated.

One version of this approach is to break the heat exchanger into many fixed length segments. However, this increases the number of control volumes or segments to be considered. Another version, the moving boundary method, uses a minimum number of control volumes (segments), the length of which vary as operating conditions change, capturing what occurs in the actual device (Gardner & Luthman, 2016). The benefit of using a lumped parameter approach to represent the VCC system is its ability to reduce the dependence on spatial coordinates and utilize ordinary differential equations, rather than rely on a much higher number of zones with fixed lengths (like an FEA approach). As mentioned in (Matko, Geiger, & Werner, 2001) this method is also useful for controller/observer design.

Observers are an extremely useful tool when it comes to monitoring what is going on within a physical system. For example, by measuring several variables that help define what is occurring within, an observer can estimate those remaining variables that may be difficult, or even impossible to measure. This information can then be used for control purposes, to simply observe performance, monitor the response of the system to various inputs, etc. However, since a model is only as good as its parameters, the purpose of this thesis is twofold: First, to identify the overall heat transfer coefficients which incorporate the fin geometry typically ignored by most controls-oriented models of this system. Then using those coefficients, calibrate a lumped parameter system model to published system performance. Second, to develop a nonlinear state observer based on the calibrated system model, which could be used to monitor a physical system. The results of this

research could be used to provide better approximations for design purposes or develop the tools necessary to monitor real-time performance in physical systems used throughout the commercial and residential industries.

For this thesis, a 2-ton Goodman residential HVAC unit utilizing the refrigerant R410a (Model: GSX130241DA, shown in Figure 4) was simulated due to its readily accessible manufacturer's data on cooling performance (Goodman Air Conditioning & Heating), as well as its intended use in future experimental validation. As such, relevant data about the system including: the high and low operating pressures, refrigerant used, heat removed from the system, and power consumed for certain operating points were readily available[1].

Figure 4. Goodman Residential Air Conditioning Unit.

In chapter 2, relevant papers referenced throughout this thesis are reviewed in order to outline the background used to develop the necessary heat transfer coefficients. Chapter 3 identifies the parameters necessary to build both the dynamic VCC model and the nonlinear observer. Chapter 4 outlines the calibration process for the heat transfer

[1] See APPENDIX A

coefficients, while chapter 5 implements the observer to predict system performance. Chapter 6 summarizes the findings of the thesis.

CHAPTER TWO: LITERATURE REVIEW

Much of the research performed in modelling VCC systems to date is primarily focused on steady-state and empirical methods. However, an increasing number of researchers have been turning their focus toward more dynamic models and simulations (Luthman, 2016).

Starting with first principles, He developed a lumped parameter model using the moving boundary approach (He, 1996). Through extensive experimental testing, this model was shown to be relatively effective at capturing the main dynamic characteristics of a VCC. Most recently, research was conducted that led to the development of a quasi-steady state model to identify the heat transfer characteristics of both the evaporator and condenser of a VCC from performance data provided by the manufacturer (Luthman, 2016). This approach utilizes the moving boundary method used by Li (2009) and various others including McKinley & Alleyne (2008), Frink (2005), and Rasmussen (2005), all of whom rely heavily on the work presented in He (1996). As such, the model presented in He (1996) is the backbone for the research presented below and is summarized in more detail to follow.

While some of the more recent research has incorporated the fins into the model of VCC systems, this was done through testing physical systems in a lab setting. Therefore, these models are specific to the unit tested. Luthman (2016) and Gardner & Luthman (2016) introduced the concept of utilizing effective heat transfer coefficients identified through performance data provided by a systems manufacturer, to incorporate

the effect of the fins throughout each heat exchanger. Utilizing these effective coefficients, could potentially eliminate the need for obtaining and testing a physical system prior to predicting the response or performance of a specific unit.

However, the steady state equations proved to be numerically ill conditioned and did not converge well. As such, much of the work presented by Luthman (2016) and Gardner & Luthman (2016) is re-evaluated throughout this thesis prior to expanding on the lumped parameter model provided by He (1996), and the implementation of a nonlinear observer to monitor performance of the system.

As described in Luthman (2016) and He (1996), a thermodynamic analysis of the heat exchangers used throughout a VCC system can be used to mathematically define the heat transfer phenomenon occurring in each. To do so, the following assumptions were made:

- The heat exchangers can be modelled as a single long tube.
- The pressure drop across each heat exchanger is negligible.
- The ambient air temperatures surrounding the evaporator and condenser are uniform.
- Due to the relatively high thermal conductivity of the tube wall (usually copper or aluminum) relative to the surrounding media, the temperature of the tube wall is assumed to be uniform in the radial direction.
- The mass flow of refrigerant is uniform through each component at steady state.

Condenser Dynamics

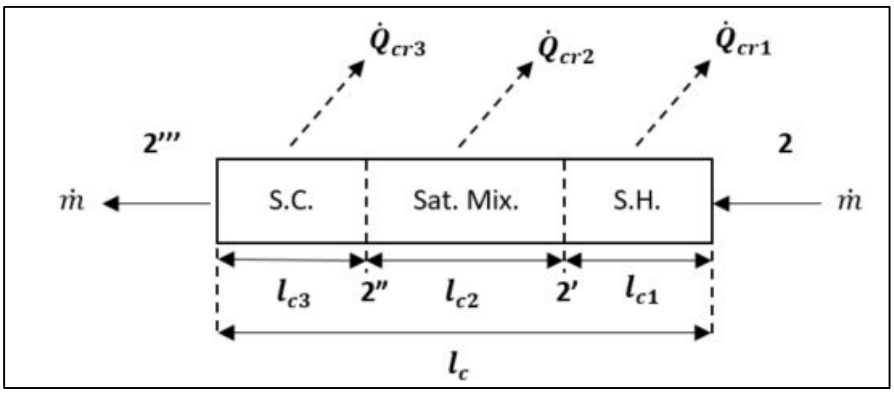

Figure 5. Condenser model layout.

Each region within the condenser can be identified and defined by the phase of the refrigerant within (superheated vapor, saturated mixture, and subcooled liquid). Starting within the superheated region, defined between states 2 and 2’ in Figure 5 above, a comparison of the energy balance and heat loss within results in Equation (1) (He, 1996).

$$\dot{m}_{ci}(h_2 - h_{2'}) + \alpha_{cr1}\pi D_{ci} l_{c1}(T_{cw1} - T_{cr1}) = 0 \quad (1)$$

Where:

$\dot{m}_{ci}$ – Is the mass flowrate into the condenser [kg/s].

h_2 – The specific enthalpy at state 2 [kJ/kg].

$h_{2'}$ – The specific enthalpy at state 2’ [kJ/kg].

α_{cr1} – The internal convection heat transfer coefficient of the refrigerant in region 1 [W/m^{2}K].

D_{ci} – The inner diameter of the condenser tubing [m].

l_{c1} – The instantaneous length of region 1 [m].

T_{cw1} – The temperature of the condenser wall in region 1 [K].

T_{cr1} – The bulk refrigerant temperature in region 1 [K].

The energy balance of the heat transfer external to the tube leads to the following equation on a per unit length basis. It is important to note that this equation assumes the heat exchanger is made up of a bare tube, rather than the actual fins that are in place.

$$\alpha_{cr1}\pi D_{ci}(T_{cr1} - T_{cw1}) + \alpha_{co1}\pi D_{co}(T_{oa} - T_{cw1}) = 0 \quad (2)$$

Where:

α_{co1} – Is the convective heat transfer coefficient for the tube in region 1 [W/m^{2}K].

D_{co} – The outer diameter of the condenser tubing [m].

T_{oa} – The free stream temperature of the outdoor air surrounding the condenser [K].

Using the same approach, the following equations can be defined for condenser region 2 (between states 2’ and 2’’) and region 3 (between states 2’’ and 2’’’) as outlined in Equations (3) – (6):

$$\dot{m}_{co}(h_{2'} - h_{2''}) + \alpha_{cr2}\pi D_{ci} l_{c2}(T_{cw2} - T_{cr2}) = 0 \quad (3)$$

$$\alpha_{cr2}\pi D_{ci}(T_{cw2} - T_{cr2}) + \alpha_{co2}\pi D_{co}(T_{oa} - T_{cw2}) = 0 \quad (4)$$

$$\dot{m}_{co}(h_{2''} - h_{2'''}) + \alpha_{cr3}\pi D_{ci} l_{c3}(T_{cw3} - T_{cr3}) = 0 \quad (5)$$

$$\alpha_{cr3}\pi D_{ci}(T_{cw3} - T_{cr3}) + \alpha_{co3}\pi D_{co}(T_{oa} - T_{cw3}) = 0 \quad (6)$$

Where:

$\dot{m}_{co}$ – Is the mass flowrate out of the condenser [kg/s].

Evaporator Dynamics

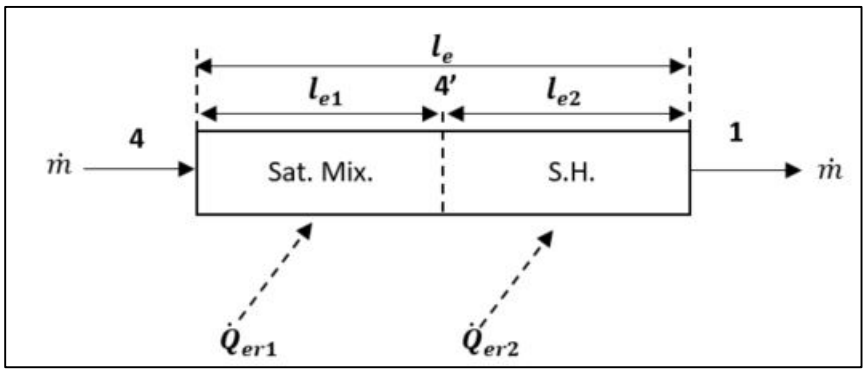

Figure 6. Evaporator model layout.

Like that of the condenser, a thermodynamic analysis (using the moving boundary method) can be used to identify energy balance within region 1 of the evaporator, resulting in Equation (7):

$$\dot{m}_{ei}(h_4 - h_{4'}) + \alpha_{er1}\pi D_{ei} l_{e1}(T_{ew1} - T_{er1}) = 0 \quad (7)$$

Where:

$\dot{m}_{ei}$ – Is the mass flowrate into the evaporator [kg/s].

h_4 – The specific enthalpy at state 4 [kJ/kg].

$h_{4'}$ – The specific enthalpy at state 4' [kJ/kg].

α_{er1} – The internal convection heat transfer coefficient of the refrigerant in region 1 [W/m^{2}K].

D_{ei} – The inner diameter of the evaporator tubing [m].

l_{e1} – The instantaneous length of region 1 [m].

T_{ew1} – The temperature of the evaporator wall in region 1 [K].

T_{er1} – The bulk refrigerant temperature in region 1 [K].

A thermodynamic analysis of the outer region of the evaporator defining region 1, can be defined as outlined below in Equation (8):

$$\alpha_{er1}\pi D_{ei}(T_{er1} - T_{ew1}) + \alpha_{eo1}\pi D_{eo}(T_{idb} - T_{ew1}) = 0 \quad (8)$$

Where:

α_{eo1} – Is the convective heat transfer coefficient for the tube in region 1 [W/m^{2}K].

D_{eo} – The outer diameter of the evaporator tubing [m].

T_{idb} – The indoor air temperature surrounding the evaporator [K].

Additionally, the following equations can be developed for region 2 within the evaporator.

$$\dot{m}_{eo}(h_{4'} - h_{4''}) + \alpha_{er2}\pi D_{ei} l_{e2}(T_{ew2} - T_{er2}) = 0 \quad (9)$$

$$\alpha_{er2}\pi D_{ei}(T_{er2} - T_{ew2}) + \alpha_{eo2}\pi D_{eo}(T_{idb} - T_{ew2}) = 0 \quad (10)$$

$\dot{m}_{eo}$ – Is the mass flowrate out of the evaporator [kg/s].

Compressor Thermodynamics

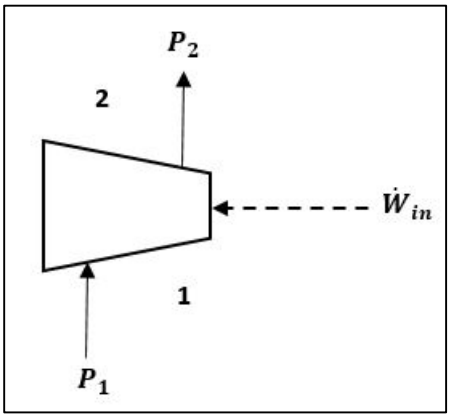

Figure 7. Compressor model layout.

The compressor in an air conditioning system takes superheated refrigerant at state 1 and compresses it to a higher pressure and temperature (state 2) prior to the refrigerant entering the condenser. Manufacturers use numerical models to predict the

performance of their compressors during different operating conditions. While these models are specific to the manufacturer, the general energy balance associated with the compressor can be defined as follows:

$$\dot{m}h_1 + \dot{W}_{in} = \dot{m}h_2 \tag{11}$$

For the research outlined in this thesis, a model of the specific compressor utilized in the Goodman unit being studied was provided by the manufacturer to provide accurate mass flow rate information, as well as power consumption. This model was assumed to provide perfect knowledge of the output from the compressor and is outlined in APPENDIX B.

Thermodynamics of the Expansion Valve

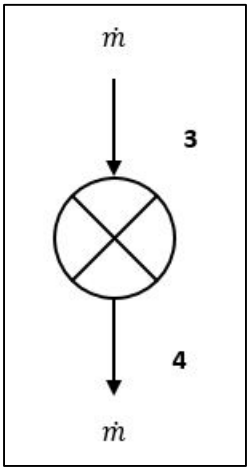

Figure 8. Expansion valve model layout.

Since the expansion valve is a throttling device, which undergoes an isenthalpic process, the high (state 3) and low-pressure states (state 4) can be related through the following relationship:

$$h_3 = h_4 \tag{12}$$

In the case of a fixed orifice expansion valve (which is the case for the Goodman system studied throughout this thesis), the mass flowrate through device can be described as in He (1996):

$$\dot{m} = C_v A_v \sqrt{\rho_3 (P_3 - P_4)} \tag{13}$$

Where:

C_v – The valve discharge coefficient.

A_v – The expansion valve area [m^2].

ρ_3 – The density of the refrigerant at state 3 [kg/m^3].

P_3 – The pressure at state 3 [Pa].

P_4 – The pressure at state 4 [Pa].

Lumped Parameter Dynamic Model & State Equations

While steady state models can be useful for estimating results, they have a limited ability to monitor a systems response when it experiences a change in input signal. Specifically, when it comes to the transient response that can be found between one steady state to the next, whereas a dynamic model can be used to track this response of the system as it moves in between.

State space models are the most powerful and dominant technique used in the analysis of engineering systems (Kulakowski, Gardner, & Shearer, 2007). These dynamic system models comprise state variables and parameters that define the state of the system. In regard to state space models, the term “state” refers to one of the variables, within a minimum set, necessary to completely describe the system at any given instant of time.

This is similar, but differs from a thermodynamic state, which is a fixed set of properties that describe the condition of a substance at that location within a system.

Once defined, the system can then take in inputs (**u**) and provide the outputs of the system (**y**) (see Figure 9 below).

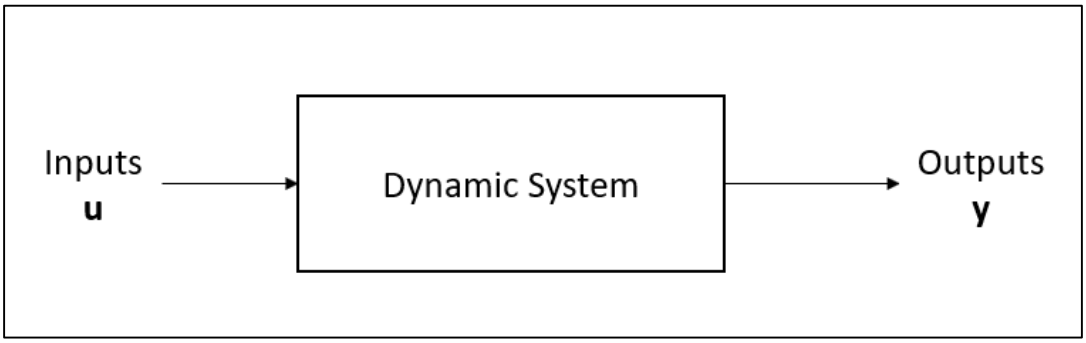

Figure 9. General dynamic model representation.

In state space form, a system can be defined as:

$$\dot{\boldsymbol{x}} = \boldsymbol{f}(\boldsymbol{x}, \boldsymbol{u}) \tag{14}$$

$$\boldsymbol{y} = \boldsymbol{g}(\boldsymbol{x}, \boldsymbol{u}) \tag{15}$$

Where:

$\boldsymbol{x}$ – Is the state vector.

$\boldsymbol{u}$ – Is the input vector.

$\boldsymbol{y}$ – Is the output vector.

In the case of the Goodman unit in question, and as illustrated in He (1996), a vector of state variables for the condenser can be defined:

$$\boldsymbol{x}_c = [L_{c1} \quad L_{c2} \quad P_c \quad h_{2'''} \quad T_{cw1} \quad T_{cw2} \quad T_{cw3}]^T \tag{16}$$

Where P_c is the condenser operating pressure. Then defining the input vector for the condenser as shown in He (1996):

$$\boldsymbol{u}_c = [\dot{m}_{ci} \quad h_2 \quad \dot{m}_{co}]^T \tag{17}$$

The state space equation for the condenser can then be simplified to:

$$\dot{\boldsymbol{x}}_c = \boldsymbol{D}_c^{-1}\boldsymbol{f}(\boldsymbol{x}_c, \boldsymbol{u}_c) \tag{18}$$

Where $\boldsymbol{f}(\boldsymbol{x}_c, \boldsymbol{u}_c)$ is defined by combining and re-arranging Equations (1) – (6) and including the mass flowrate relationship for the condenser:

$$\boldsymbol{f}(\boldsymbol{x}_c, \boldsymbol{u}_c) = \begin{bmatrix} \dot{m}_{ci}(h_2 - h_{2'}) + \alpha_{cr1}\pi D_{ci} l_{c1}(T_{cw1} - T_{cr1}) \\ \dot{m}_{co}(h_{2'} - h_{2''}) + \alpha_{cr2}\pi D_{ci} l_{c2}(T_{cw2} - T_{cr2}) \\ \dot{m}_{co}(h_{2''} - h_{2'''}) + \alpha_{cr3}\pi D_{ci} l_{c3}(T_{cw3} - T_{cr3}) \\ \dot{m}_{ci} - \dot{m}_{co} \\ \alpha_{cr1}\pi D_{ci}(T_{cr1} - T_{cw1}) + \alpha_{co1}\pi D_{co}(T_{oa} - T_{cw1}) \\ \alpha_{cr2}\pi D_{ci}(T_{cw2} - T_{cr2}) + \alpha_{co2}\pi D_{co}(T_{oa} - T_{cw2}) \\ \alpha_{cr3}\pi D_{ci}(T_{cw3} - T_{cr3}) + \alpha_{co3}\pi D_{co}(T_{oa} - T_{cw3}) \end{bmatrix} \tag{19}$$

$\boldsymbol{D}_c$ is a matrix of partial derivatives, which is defined along with its components in the literature, see He (1996).

Similarly, defining a vector of state variables for the evaporator:

$$\boldsymbol{x}_e = [L_{e1} \quad P_e \quad h_1 \quad T_{ew1} \quad T_{ew2}]^T \tag{20}$$

Where P_e is the evaporator operating pressure. Then defining the input vector for the evaporator:

$$\boldsymbol{u}_e = [\dot{m}_{ei} \quad h_3 \quad \dot{m}_{eo}]^T \tag{21}$$

Thus:

$$\dot{\boldsymbol{x}}_e = \boldsymbol{D}_e^{-1}\boldsymbol{f}(\boldsymbol{x}_e, \boldsymbol{u}_e) \tag{22}$$

Where $\boldsymbol{f}(\boldsymbol{x}_e, \boldsymbol{u}_e)$ is defined by combining and re-arranging Equations (7) – (10) and including the mass flowrate relationship for the evaporator:

$$\boldsymbol{f}(\boldsymbol{x}_e, \boldsymbol{u}_e) = \begin{bmatrix} \dot{m}_{ei}(h_4 - h_{4'}) + \alpha_{er1}\pi D_{ei} l_{e1}(T_{ew1} - T_{er1}) \\ \dot{m}_{eo}(h_{4'} - h_{4''}) + \alpha_{er2}\pi D_{ei} l_{e2}(T_{ew2} - T_{er2}) \\ \dot{m}_{ei} - \dot{m}_{eo} \\ \alpha_{er1}\pi D_{ei}(T_{er1} - T_{ew1}) + \alpha_{eo1}\pi D_{eo}(T_{idb} - T_{ew1}) \\ \alpha_{er2}\pi D_{ei}(T_{er2} - T_{ew2}) + \alpha_{eo2}\pi D_{eo}(T_{idb} - T_{ew2}) \end{bmatrix} \quad (23)$$

$\boldsymbol{D}_e$ is a matrix of partial derivatives, which is defined along with its components in the literature, see He (1996).

Observer Design

When controlling physical systems, it is often necessary to know the values of the states that define the response of the system. However, it is not always practical or even possible to measure every state. This is where state observers become very useful. State observers are used to estimate the value of state variables throughout a physical system when they cannot be measured directly. By measuring the input and a subset of the states (those that can be measured), an observer will estimate all of the state variables that define the system. The estimates of the measured states are compared to the actual measurements and that error is used to drive the observer to the correct estimates (Oppenheim & Verghese, 2010). Figure 10 below represents the general layout of a state observer.

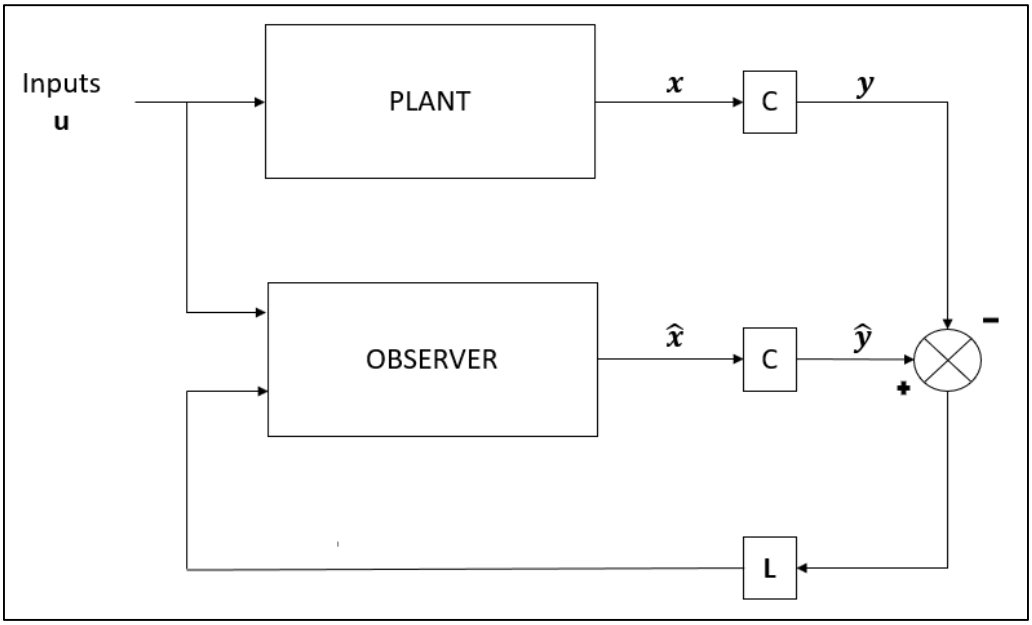

Figure 10. General Observer Schematic

Considering the general state space system described in Equations (14) and (15), an observer can be defined as:

$$\dot{\hat{\boldsymbol{x}}} = \boldsymbol{f}(\hat{\boldsymbol{x}}, \boldsymbol{u}) + \boldsymbol{L}(\boldsymbol{y} - \hat{\boldsymbol{y}}) \tag{24}$$

$$\hat{\boldsymbol{y}} = \boldsymbol{g}(\hat{\boldsymbol{x}}, \boldsymbol{u}) \tag{25}$$

Where:

$\hat{\boldsymbol{x}}$ – is a vector of the estimated states

$\hat{\boldsymbol{y}}$ – is the estimated output vector

$\boldsymbol{L}$ – is the observer gain matrix

Cheng (2002) proposed utilizing nonlinear state observers to estimate the important, but immeasurable, state variables necessary for stringent control of VCC systems. Furthermore, Cheng, Asada, He, & Kasahara (2005) showed good convergence (utilizing methods outlined by Lhomiller & Slotine (1998) to a physical system by using observers to estimate the heat transfer rate and length of the two-phase regions for both an evaporator and condenser.

Thesis Contributions

While much of the research discussed above drastically improved the collective ability to model a VCC system, they neglect to capture the effect fins within the heat exchangers contribute to the system. This thesis builds upon the work of those referenced by identifying overall heat transfer coefficients to capture this effect. These coefficients, along with the complete dynamic model, form the basis of a nonlinear state observer which can be used to further designers and technician's ability to accurately predict & monitor system performance.

CHAPTER THREE: DYNAMIC MODEL PARAMETER IDENTIFICATION

As outlined above, a dynamic lumped parameter model for a VCC system is well defined. However, the majority of these models still rely on the assumption that the heat exchangers behave as if they were a long, bare tube, and very little has been done to capture the fins contributions to the system when applied to controls-oriented models. While there are various finite element models that can evaluate the performance of the fins, these models take much too long to evaluate to be used in a controls type setting.

Gardner & Luthman (2016) and Luthman (2016) proposed that effective heat transfer coefficients can be developed from performance data provided by the manufacturer. These coefficients can then be used to capture the effect of the fins.

Parameter Identification Based on System Data:

By assuming that the heat transfer characteristics for the fins are relatively constant regardless of their location throughout the heat exchanger (due to the consistency of the fins construction pattern and geometry), an overall fin heat transfer coefficient (UA'_{fc}) can be defined for the condenser. Similarly, an overall fin heat transfer coefficient (UA'_{fe}) can be defined for the evaporator. Where A'_f can be considered an effective heat transfer area per unit length of the heat exchanger and U is the effective convection coefficient across the outer portion of the entire heat exchanger. For the purposes of this work, these individual components (U & A'_f) were lumped together into a single parameter, one for each heat exchanger (UA'_{fc} & UA'_{fe}). This effective value can then be used to approximate the contribution the fins have within each heat exchanger,

rather than relying on just the model of a bare tube throughout. While this substitution is not necessarily an exact equivalence, it can be used as a tuning mechanism for accurately representing the system.

By replacing the portions of equations (19) & (23) that rely on the bare tube assumption with these effective heat transfer coefficients, a new set of equations to model the condenser and evaporator, that account for the fins throughout, can be defined as follows:

$$\boldsymbol{f}(\boldsymbol{x}_c, \boldsymbol{u}_c) = \begin{bmatrix} \dot{m}_{ci}(h_2 - h_{2'}) + \alpha_{cr1}\pi D_{ci} l_{c1}(T_{cw1} - T_{cr1}) \\ \dot{m}_{co}(h_{2'} - h_{2''}) + \alpha_{cr2}\pi D_{ci} l_{c2}(T_{cw2} - T_{cr2}) \\ \dot{m}_{co}(h_{2''} - h_{2'''}) + \alpha_{cr3}\pi D_{ci} l_{c3}(T_{cw3} - T_{cr3}) \\ \dot{m}_{ci} - \dot{m}_{co} \\ \alpha_{cr1}\pi D_{ci}(T_{cr1} - T_{cw1}) + UA'_{fc}(T_{oa} - T_{cw1}) \\ \alpha_{cr2}\pi D_{ci}(T_{cw2} - T_{cr2}) + UA'_{fc}(T_{oa} - T_{cw2}) \\ \alpha_{cr3}\pi D_{ci}(T_{cw3} - T_{cr3}) + UA'_{fc}(T_{oa} - T_{cw3}) \end{bmatrix} \tag{26}$$

$$\boldsymbol{f}(\boldsymbol{x}_e, \boldsymbol{u}_e) = \begin{bmatrix} \dot{m}_{ei}(h_4 - h_{4'}) + \alpha_{er1}\pi D_{ei} l_{e1}(T_{ew1} - T_{er1}) \\ \dot{m}_{eo}(h_{4'} - h_{4''}) + \alpha_{er2}\pi D_{ei} l_{e2}(T_{ew2} - T_{er2}) \\ \dot{m}_{ei} - \dot{m}_{eo} \\ \alpha_{er1}\pi D_{ei}(T_{er1} - T_{ew1}) + UA'_{fe}(T_{idb} - T_{ew1}) \\ \alpha_{er2}\pi D_{ei}(T_{er2} - T_{ew2}) + UA'_{fe}(T_{idb} - T_{ew2}) \end{bmatrix} \tag{27}$$

These new sets of equations highlight the parameters necessary to represent the system as a whole. Specifically, the internal convection coefficients of the refrigerant in each heat exchanger (α_{cr} & α_{er}), and the new effective heat transfer coefficients (UA'_{fc} & UA'_{fe}).

Starting with the coefficients on the inside of the tubes, the convective heat transfer coefficient for the refrigerant within region 1 and region 3 of the condenser can be defined by the Dittus-Boelter equation for cooling as illustrated by Frink (2005):

$$\alpha_{cr1} = 0.023\left(\frac{k}{D_{ci}}\right)Re^{0.8}Pr^{0.3} \quad (28)$$

$$\alpha_{cr3} = 0.023\left(\frac{k}{D_{ci}}\right)Re^{0.8}Pr^{0.3} \quad (29)$$

Where:

k - Is the thermal conductivity of the refrigerant within the region [W/m-K]

$Re = \frac{\dot{m}D}{A\mu}$ – Is the Reynolds Number

$Pr = \frac{\mu c_p}{k}$ – Is the Prandtl Number

μ – is the absolute viscosity of the refrigerant [kg/m-s]

c_p – is the thermal capacity of the refrigerant [J/K]

The convective heat transfer coefficient for region 2 within the condenser is defined in (30) as illustrated by He (1996). This differs from (28) & (29) because it is condensing heat transfer within the mixed region of the condenser:

$$\alpha_{cr2} = \frac{k\,Nu}{D_{ci}} \quad (30)$$

Where:

$Nu = \frac{Re^{0.9}PrF_1{}^{\beta}}{F_2}$ – Is the Nusselt Number

$F_1 = 0.15(X_{tt}^{-1} + 2.85X_{tt}^{0.524})$

$\beta = 1$ for $F_1 \leq 1$, $\beta = 1.15$ for $F_1 > 1$

$F_2 = 5Pr + 5ln(1 + Pr) + 2.5ln(0.0313Re^{0.812})$

$X_{tt} = \left(\frac{1-x}{x}\right)^{0.9}\left(\frac{v_l}{v_v}\right)^{0.5}\left(\frac{\mu_l}{\mu_v}\right)^{0.1}$

x – Is the average quality of the refrigerant throughout the region

v_l – Is the specific volume of the liquid refrigerant [m^3/kg]

v_v – Is the specific volume of the refrigerant vapor [m^3/kg]

μ_l – Is the absolute viscosity of the liquid refrigerant [kg/m-s]

μ_v – Is the absolute viscosity of the refrigerant vapor [kg/m-s]

For the evaporator, as defined by Smith, Wattelet, & Newell (1993), the convective heat transfer coefficient for the refrigerant within region 1 (evaporative heat transfer within the mixed region) can be defined as:

$$\alpha_{er1} = 0.00097\left(\frac{k_l}{D}\right) Re \left(\frac{\Delta x h_{fg}}{gL}\right)^{0.5} \tag{31}$$

Where:

Δx – Is the change in quality across the region

h_{fg} – Is the latent heat of vaporization of the refrigerant [kJ/kg]

g – Is the acceleration of gravity [m/s^2]

L – Is the length of the heat exchanger tubing [m]

The convective heat transfer coefficient for the refrigerant within region 2 of the evaporator can be defined by the Dittus-Boelter equation for heating as illustrated by Frink (2005):

$$\alpha_{er2} = 0.023\left(\frac{k}{D}\right) Re^{0.8} Pr^{0.4} \tag{32}$$

Note that each of these internal heat transfer coefficients are dependent on the refrigerant properties at that instance in time and are calculated along with each iteration of the dynamic model. Once the convective heat transfer parameters are considered, the values of UA'_{fc} and UA'_{fe} can be evaluated using the manufacturer's data on unit performance and solving a set of nonlinear algebraic equations, however this proved to be ill-conditioned (as illustrated by Luthman (2016) & Gardner & Luthman (2016)) and

further highlighted the sensitivity of each coefficient to the environment around the heat exchanger. To overcome the numerical difficulties, the dynamic simulation of the system (defined in the following chapter) was used to find best fit expressions for each coefficient associated with the Goodman unit studied throughout this thesis.

CHAPTER FOUR: DYNAMIC MODEL AND CALIBRATION

To simulate the 2-ton Goodman air conditioning unit studied throughout this thesis, MATLAB was used as the primary computing environment. Simulating was performed within Simulink, MATLAB's simulation environment. Refrigerant properties necessary to solve for system parameters, and thermodynamic states around the VCC were obtained via CoolProp (Bell, Wronski, Quoilin, & Lemort, 2014). CoolProp is a C++ library that can be accessed via various MATLAB commands to evaluate various fluid state properties for given conditions. More information can be accessed at www.coolprop.org.

Model Development

As outlined in Chapter 2, the various components of a VCC system can be modelled via a state space approach. By combining the work outlined in Luthman (2016) & He (1996), and leveraging the modified condenser and evaporator equations (26) & (27), a dynamic simulation of the 2-ton Goodman unit was created (shown in Figure 11).

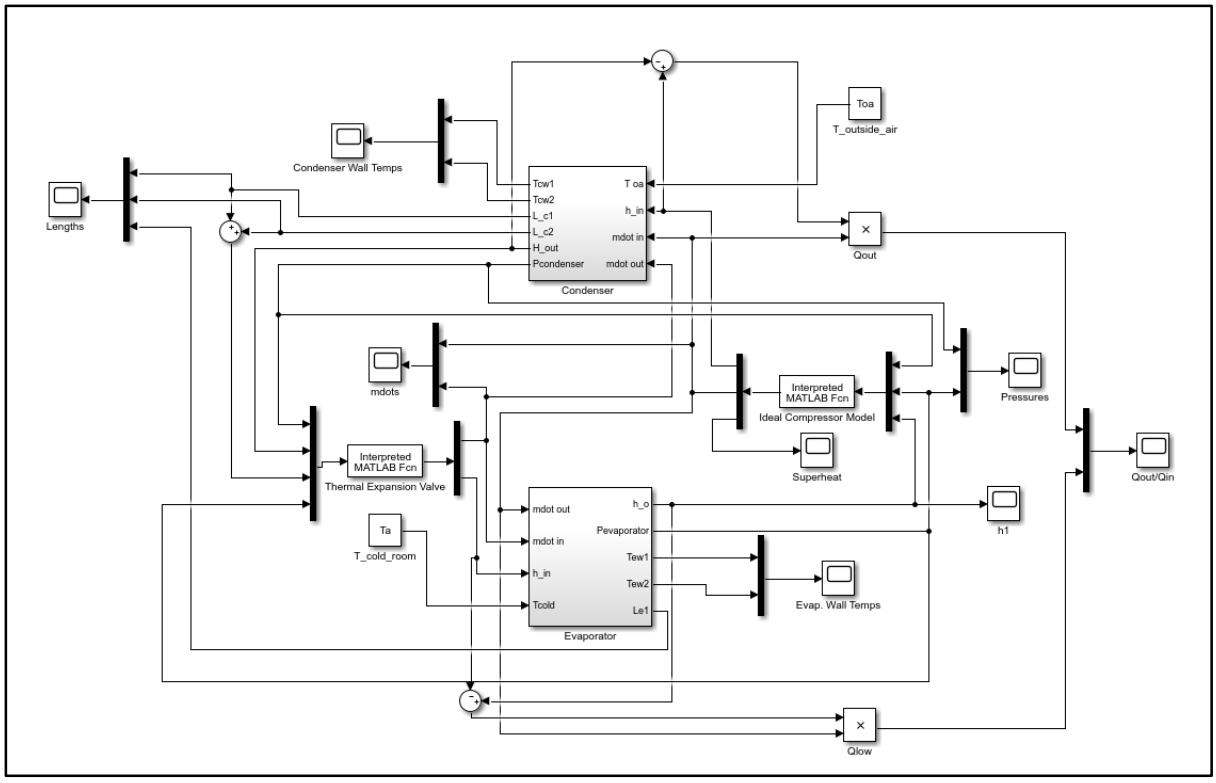

Figure 11. Simulink Model of VCC System.

This simulation takes in set points for the outdoor air temperature and the ambient room temperature, then evaluates the states throughout each heat exchanger for a given time set.

Parameter Identification for Effective Fin Coefficients (UA')

To identify the values for UA'_{fc} and UA'_{fe} initial estimates were calculated using the steady state performance values from the manufacturer as tabulated in (Goodman Air Conditioning & Heating). Since these effective heat transfer coefficients are not directly related to first principles, they were then adjusted such that the heat removed from the system calculated by the model matched the tabulated results for the physical system at the corresponding set point (recreated the manufacturers' test data). See Table 2 and Table 3 below.

Table 2. Heat Removed by Model Compared to Literature.

			Outdoor Ambient Air Temperature (F)							
			65				75			
			Entering Indoor Wet Bulb Temperature (F)							
Tidb (F)	Airflow		59	63	67	71	59	63	67	71
70	800	Qlow - Literature (W)	6418	6653	7268	-	6272	6506	7122	-
		Qlow - Model (W)	6418	6653	7268	-	6272	6506	7122	-
		% Error	0.00%	0.00%	0.00%	-	0.00%	0.00%	0.00%	-
75	800	Qlow - Literature (W)	6535	6711	7268	7796	6360	6565	7092	7620
		Qlow - Model (W)	6535	6711	7268	7796	6360	6565	7092	7620
		% Error	0.00%	0.00%	0.00%	0.00%	0.00%	0.00%	0.00%	0.00%

Table 3. Example Effective Coefficients Sets

Tibd (F)	Toa (F)	Tiwb (F)	Uafc	Uafe	Tiwb (F)	Uafc	Uafe	Tiwb (F)	Uafc	Uafe	Tiwb (F)	Uafc	Uafe
70	65	59	15.3863	73.35	63	15.3863	82.15	67	15.3863	123.3	71	-	-
70	75	59	17.8267	72.32	63	17.8267	80.35	67	17.8267	117	71	-	-
75	65	59	15.3863	59.66	63	15.3863	63.73	67	15.3863	81.5	71	15.3863	113.2
75	75	59	17.8267	58.05	63	17.8267	62.35	67	17.8267	77.33	71	17.8267	103.65

Table 2 compares the performance data provided by the manufacturer (see APPENDIX A) to the performance estimated by the dynamic model using the effective coefficient pair (from Table 3) for a given set point. For example, the manufacturer states that the 2-ton Goodman unit will remove heat from the target environment at a rate of 6.653 kW when operating with an outdoor temperature of 65°F, indoor setpoint temperature of 70°F, and indoor wet bulb temperature of 63°F. The effective heat transfer coefficients for were adjusted until the dynamic model estimated the correct heat removal rate of 6.653 kW.

This was repeated for the remaining conditions for the 70°F and 75°F set points (airflow of 600) to identify the coefficient pairs that recreated the performance recorded by the manufacturer. During this process, it became clear that UA'_{fc} was a function of the outdoor air temperature. Similarly, UA'_{fe} was found to be a function of both the dry bulb and wet bulb temperature of the air surrounding the heat exchanger (shown below).

$$UA'_{fc} = f(T_{oa})$$

$$UA'_{fe} = f(T_{idb}, T_{iwb})$$

After regressing the evaporator coefficients to their associated set point, the average result for each coefficient (UA'_{fc} & UA'_{fe}) were plotted relative to the range of conditions as shown in Figure 12 and Figure 13 below.

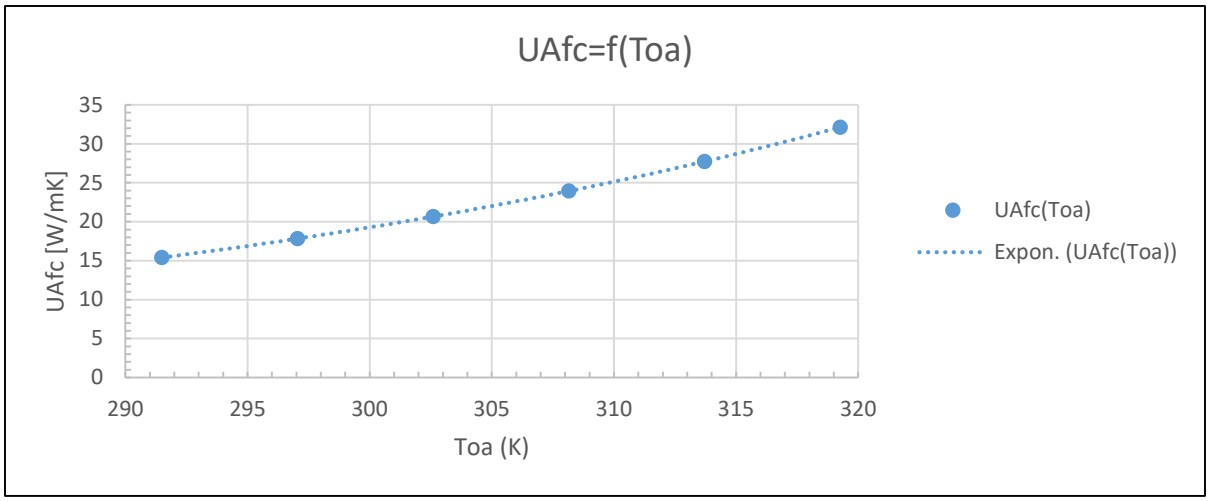

Figure 12. Effective Condenser Fin Coefficient.

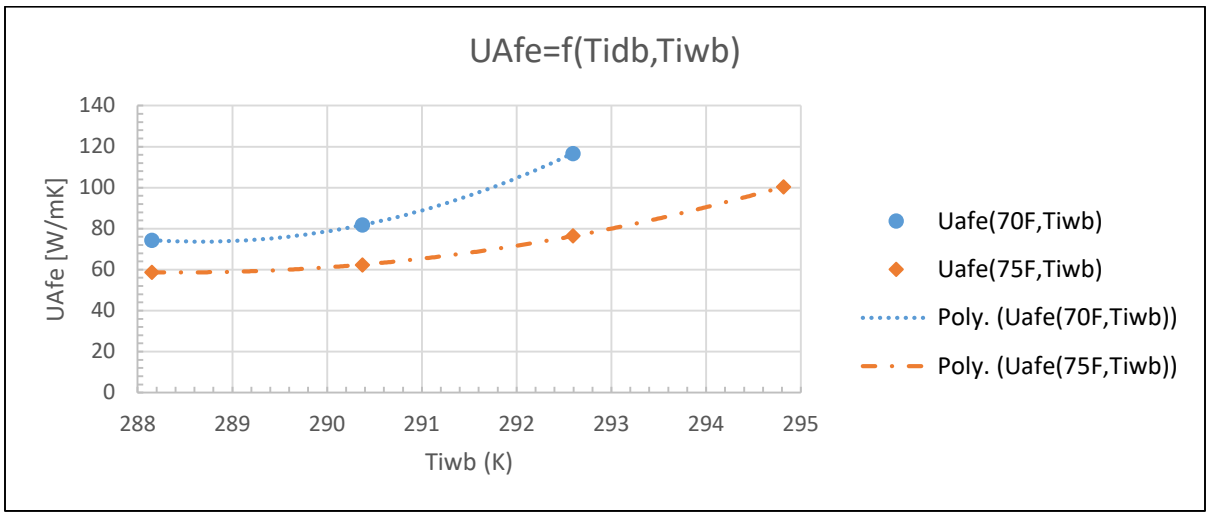

Figure 13. Effective Evaporator Fin Coefficient.

Note the two different curves shown in Figure 13, represent the coefficient profile for the evaporator at two different set point temperatures. Using curve fitting tools in excel, the following expressions were derived for each coefficient.

$$UA'_{fc} = 0.0068e^{0.0265T_{oa}} \quad (33)$$

$$UA'_{fe} = AT_{iwb}{}^{2} - BT_{iwb} + C \quad (34)$$

Where:

Table 4. UA'_{fe} Coefficients

$\boldsymbol{T_{idb}}$ (K)	A$\left[\frac{\boldsymbol{W}}{\boldsymbol{mK^3}}\right]$	B $\left[\frac{\boldsymbol{W}}{\boldsymbol{mK^2}}\right]$	C $\left[\frac{\boldsymbol{W}}{\boldsymbol{mK}}\right]$
294.26 (70°F)	2.79	1,609.25	232,340.42
297.04 (75°F)	1.039	596.87	86,144

For the condenser, an exponential expression dependent on the ambient outdoor air temperature was developed to describe UA'_{fc}. Whereas for the evaporator, a polynomial fit that utilizes different sets of coefficients dependent on the set point temperature ($\boldsymbol{T_{idb}}$), then relies on the wet-bulb temperature of the air surrounding to identify UA'_{fe}.

Using equations (33) & (34) in the dynamic model shown above resulted in minimal error (within +3.73% & -2.12% as compared to the published data provided by the manufacturer) when predicting the heat removed by the system as shown in Table 5 and Table 6 below.

Table 5. Dynamic Model Results Outdoor Air Temp. Range 65 °F – 85 °F

			Outdoor Ambient Air Temperature (F)											
			65				75				85			
			Entering Indoor Wet Bulb Temperature (F)											
Tidb (F)	Airflow		59	63	67	71	59	63	67	71	59	63	67	71
70	800	Qlow - Literature (W)	6418	6653	7268	-	6272	6506	7122	-	6125	6330	6946	-
		Qlow - Model (W)	6449	6645	7203	-	6338	6542	7119	-	6159	6371	6961	-
		% Error	0.48%	-0.12%	-0.89%	-	1.05%	0.55%	-0.04%	-	0.56%	0.65%	0.22%	-
75	800	Qlow - Literature (W)	6535	6711	7268	7796	6360	6565	7092	7620	6213	6389	6916	7444
		Qlow - Model (W)	6491	6658	7136	7631	6395	6569	7065	7573	6235	6417	6925	7441
		% Error	-0.67%	-0.79%	-1.82%	-2.12%	0.55%	0.06%	-0.38%	-0.62%	0.35%	0.44%	0.13%	-0.04%

Table 6. Dynamic Model Results Outdoor Air Temp. Range 95 °F – 115 °F

			Outdoor Ambient Air Temperature (F)											
			95				105				115			
			Entering Indoor Wet Bulb Temperature (F)											
Tidb (F)	Airflow		59	63	67	71	59	63	67	71	59	63	67	71
70	800	Qlow - Literature (W)	5979	6184	6770	-	5656	5861	6448	-	5246	5451	5949	-
		Qlow - Model (W)	5913	6133	6732	-	5600	5830	6435	-	5226	5466	6075	-
		% Error	-1.10%	-0.82%	-0.56%	-	-0.99%	-0.53%	-0.20%	-	-0.38%	0.28%	2.12%	-
75	800	Qlow - Literature (W)	6067	6242	6770	7268	5774	5920	6418	6887	5334	5510	5949	6389
		Qlow - Model (W)	6015	6202	6720	7236	5736	5930	6453	6964	5409	5607	6130	6627
		% Error	-0.86%	-0.64%	-0.74%	-0.44%	-0.66%	0.17%	0.55%	1.12%	1.41%	1.76%	3.04%	3.73%

While testing the dynamic model, it was discovered that the CoolProp library is somewhat limited in its ability to predict properties within the saturated region for non-pure substances (R410a in this case). This makes the model sensitive and prone to fail when stepping from one set point to another, however it did not impact convergence to steady state for a single set point.

CHAPTER FIVE: OBSERVER IMPLEMENTATION

The most common application of state observers is in the context of state feedback control. In many situations, it is either impossible (or highly impractical) to measure every state that defines the system. In these instances, an observer can be used to estimate all of the states by only measuring a select few. The observer then compares the estimated state to the "actual" (measured) value and adjusts as necessary to converge on the true output of the system.

For the purposes of this research, the dynamic model described in the previous chapter was used as the "plant" or representation of the Goodman unit studied. A nonlinear observer was then created using a second version of the dynamic model with different initial conditions to test the observer's ability to converge on estimates of system performance utilizing the effective heat transfer coefficients defined for each heat exchanger. While this simplification provided a useful tool for developing the observer, further testing should be performed using the actual physical system.

Measured States for the Condenser

Recall the states used to model the condenser (from equation (16)) include; the lengths of superheated and saturated regions, the pressure throughout the heat exchanger, the specific enthalpy leaving the condenser, and the wall temperatures of the tubing throughout each region. These seven state variables provide the minimum set of information necessary to fully understand the dynamics of the condenser, however measuring all seven states would be nearly impossible. For example, measuring the

lengths of each region within the heat exchanger would be very difficult to accomplish, and measuring the specific enthalpy directly would be impossible. This leaves the pressure and wall temperatures to be considered as likely measurements to be used when linking the observer to the physical system.

Since nearly all residential air conditioning systems (like the Goodman unit studied) have easily accessible pressure ports for their heat exchangers (see Figure 14), a simple pressure transducer could be utilized to monitor the condenser pressure.

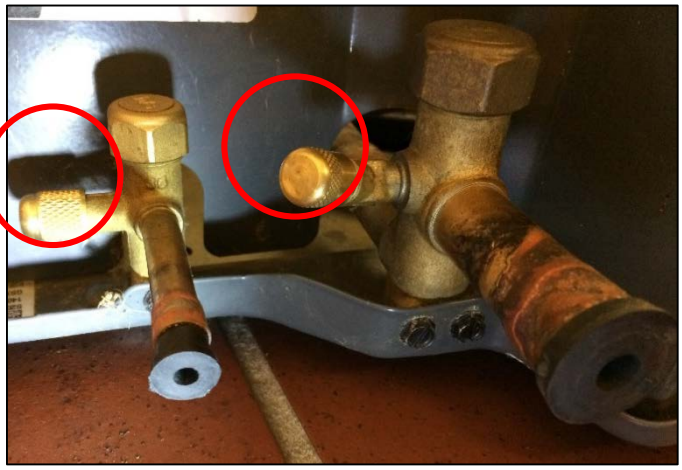

Figure 14. Existing pressure ports on 2-ton Goodman unit.

Considering the low cost and ease of implementation of temperature transducers, measuring the condenser tubing wall temperatures throughout the heat exchanger can also be accomplished easily. However, to reduce the number of sensors present, only the wall temperature for the saturated region of the condenser was selected as a measured state (rather than measuring three wall temperatures) since most of the heat transfer from the system occurs throughout this area. Therefore, the two measurements for the condenser, used by the observer, include the pressure and the wall temperature of the saturated region.

Measured States for the Evaporator

The states identified for the evaporator (from equation (20)) include; the length of the saturated region, the pressure throughout the heat exchanger, the specific enthalpy leaving the evaporator, and the wall temperatures of the tubing through each region. Like the condenser, the pressure and wall temperature within the saturated region (highest concentration of heat transfer to the system) were selected as the states to be measured to be used within the observer.

Nonlinear Observer Implementation

As shown in Figure 15 and Figure 16 below, the states outlined above were directly measured from the dynamic model while implementing the 4-measurement nonlinear observer.

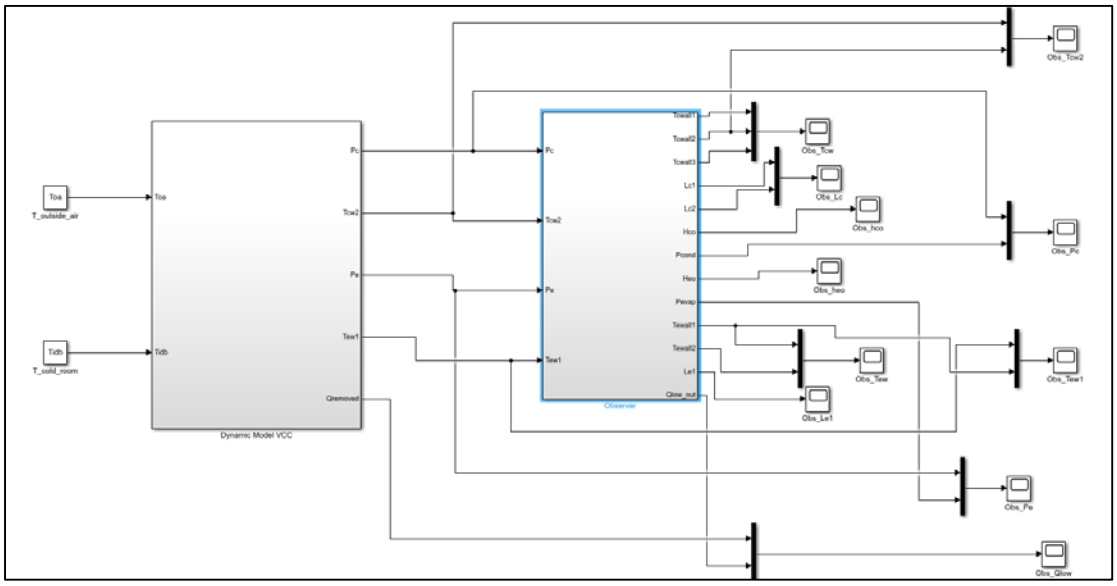

Figure 15. Four measurement observer model.

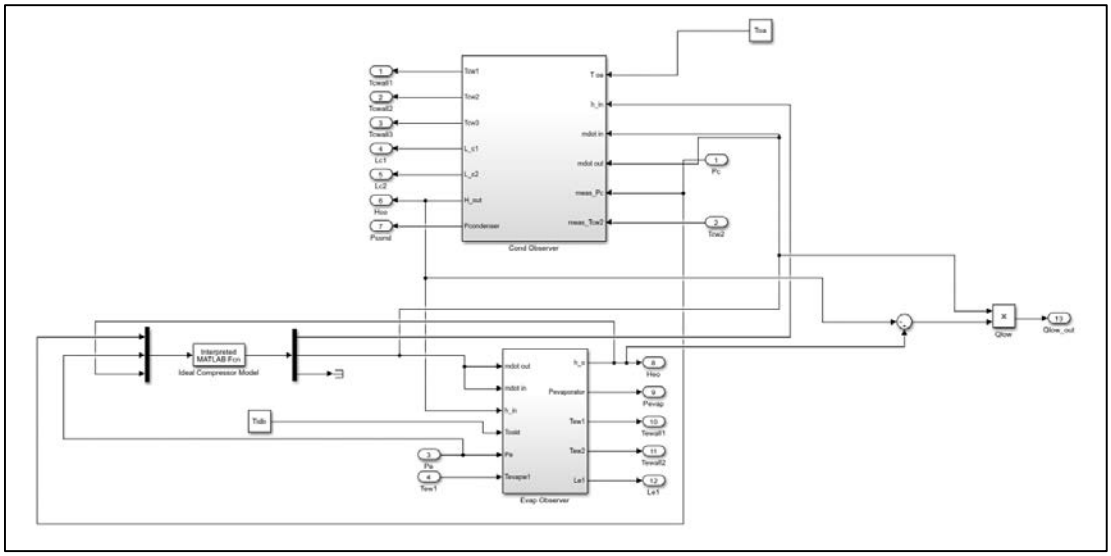

Figure 16. Inside observer block of the four-measurement observer.

Initial conditions for the observer were set to the steady state result of the dynamic model after simulating the Goodman unit at a different set point to ensure defined initial conditions. Gain values for the measured states (shown in Table 7) were selected to provide stable solutions and to converge quickly to those simulated by the dynamic model (See APPENDIX C

for convergence of measured states).

Table 7. Nonlinear State Observer Gain Values

State Measured	Gain Value Applied
P_c	0.25
T_{cw2}	0.025
P_e	10
T_{ew1}	1

As shown in Figure 17, the observer was able to provide a good estimate of the heat removed by the system (represented by dotted profile) when compared to the steady

state published performance (represented by the solid line). This also showed quick convergence to within 2% error after only 20 seconds of simulation and full agreement (less than 0.1% error) within roughly 90 seconds.

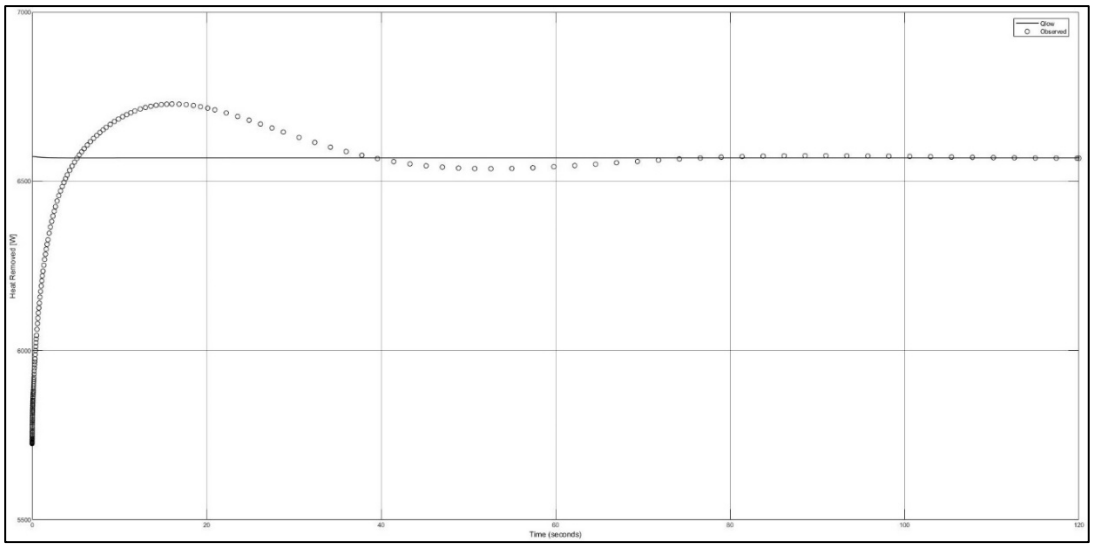

Figure 17. 4-measurement observer convergence for heat removed from system.

To attempt to further reduce the number of measurements necessary, a second observer was created that excludes the wall temperatures utilized in the 4-measurement observer. This two-measurement nonlinear observer (shown below) relies on only the pressures of each heat exchanger.

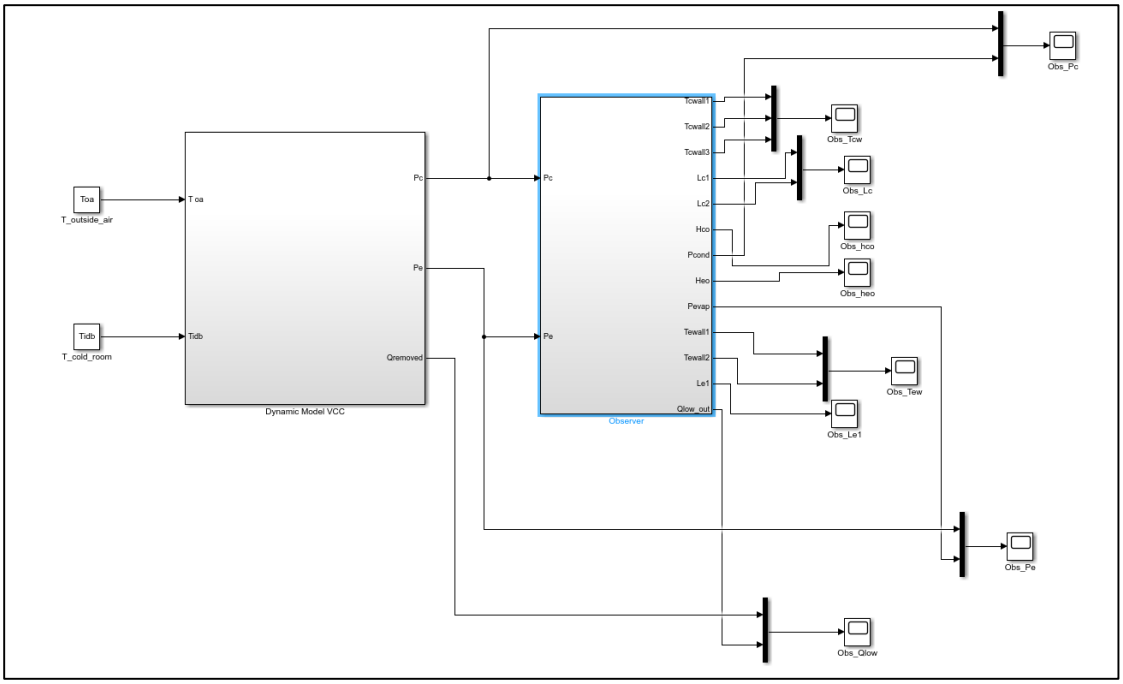

Figure 18. Two-measurement observer model.

Figure 19, below, shows the convergence of the two-measurement observer's prediction of the heat removed from the system as compared to that of the dynamic model. Again, the dotted profile represents the estimate from the observer of the heat removed by the system, and the solid line represents the published steady state performance for that set of conditions.

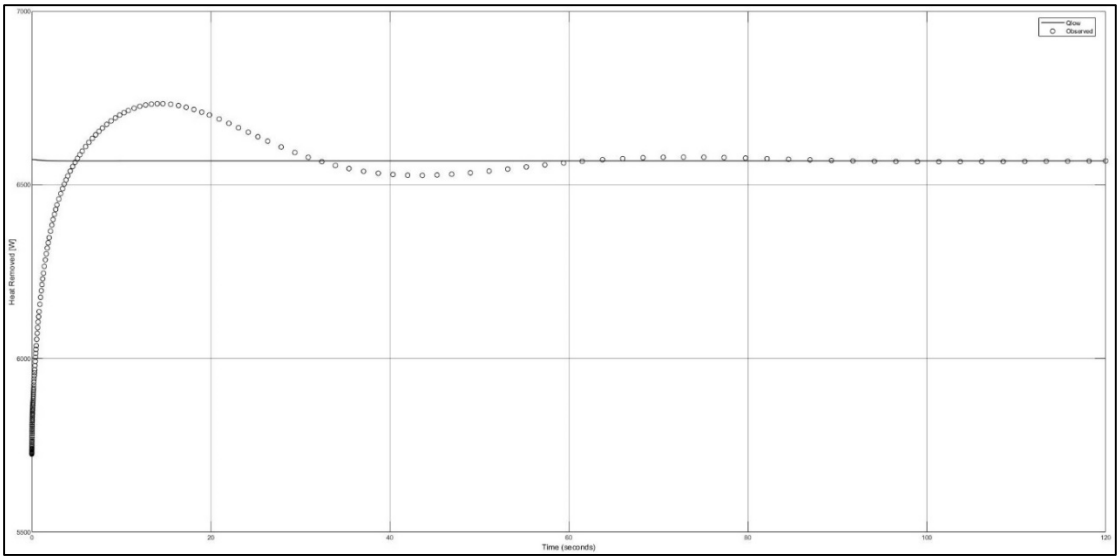

Figure 19. 2-Measurement observer convergence for heat removed from system.

Figure 20 shows the convergence time and profile for each of the four states measured by the observer. These included the pressures of each heat exchanger, as well as the wall temperatures within each saturated region as well.

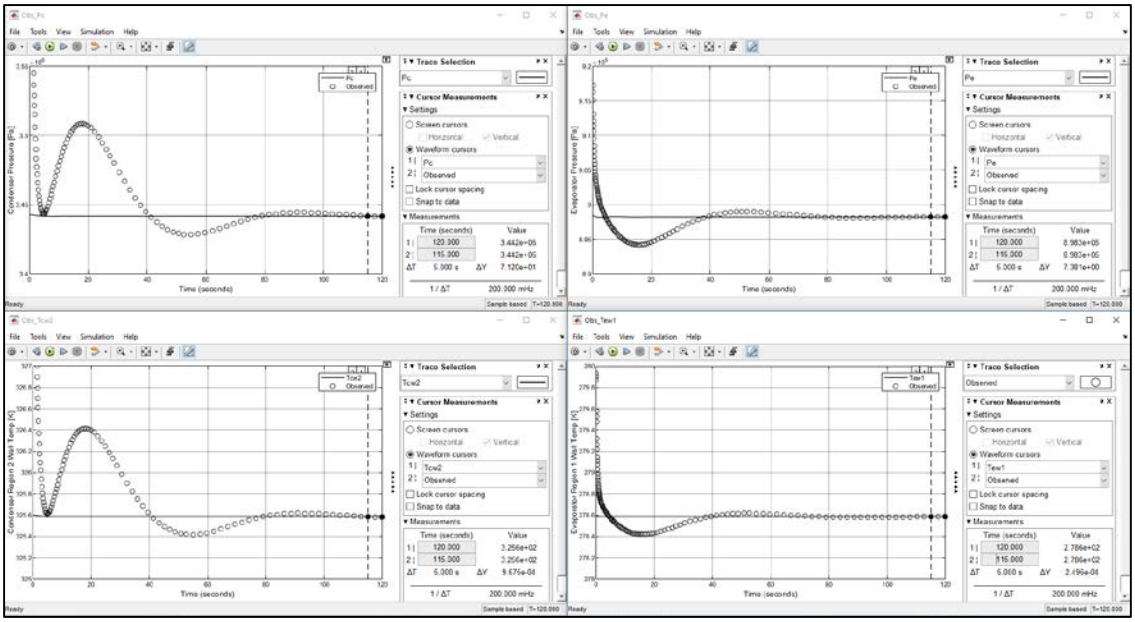

Figure 20. 4-Measurement observer convergence time comparison.

Removing the measurement of the wall temperatures showed very similar convergence times for the heat removed by the system. A closer inspection of the

measured (and estimated) states showed that the 2-measurement observer took roughly 5 seconds longer (simulated time) to converge than the response of the 4-measurement observer. This can be seen by comparing Figure 20 to Figure 21 below. Figure 21 illustrates the convergence time and profile for both of the measured states (the pressures of each heat exchanger), as well as the estimated state response for each saturated region wall temperature.

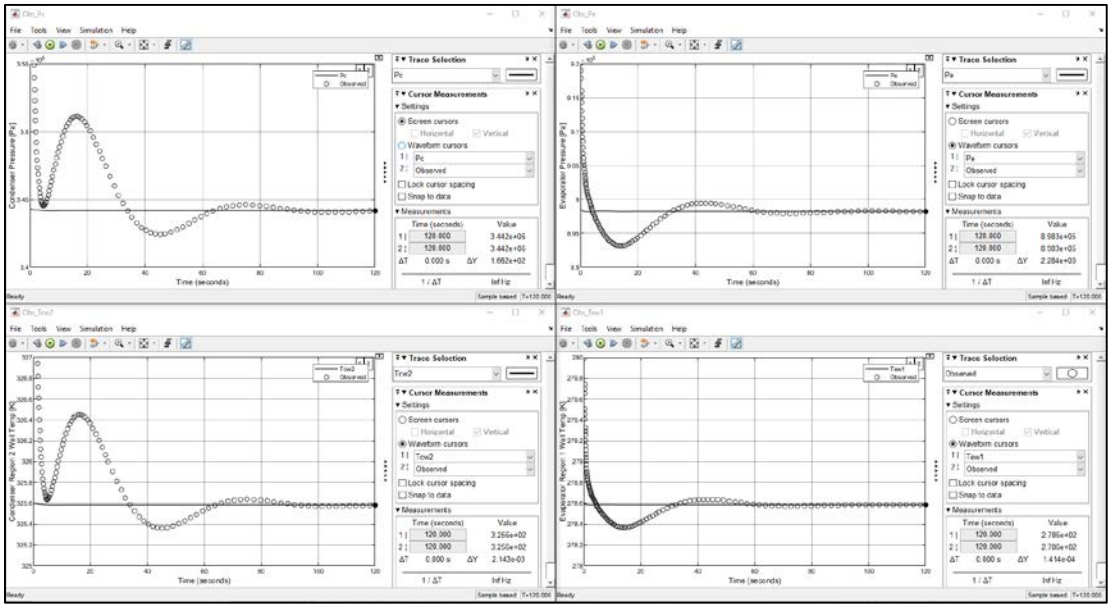

Figure 21. 2-Measurement observer convergence time comparison.

An additional 2-measurement observer (measuring both wall temperatures), was also tested. However, this version remained unstable for all gain values attempted indicating that at least one pressure measurement is necessary to converge on the final solution. This is likely due (in part) to the pressure being a state variable that can also be used to help define the thermodynamic state of the refrigerant at that location. Whereas the wall temperatures cannot be used to define a thermodynamic state of the refrigerant directly.

Finally, a 3-measurement observer was created, but did not improve upon the results from the 2-measurement (measuring both pressures) observer. This indicates that measuring both pressures as well as a wall temperature within each heat exchanger (the 4-measurement observer) provides the fastest convergence to the output of the plant and would be the recommended starting point for testing with a physical system.

CHAPTER SIX: CONCLUSION

With more and more reliance on simulation to reduce the need for repetitive prototyping, continually improving our ability to model and predict the behavior of physical systems is key. This thesis adds to this ability by improving upon well-defined models of VCC systems, which rely on simplified geometry, to include the effect fins have within the heat transfer surrounding the systems heat exchangers. Having the ability to monitor performance in real-time, technicians & engineers could improve the reliability of VCC systems and improve energy efficiency by fine tuning operating conditions to suit. As such, utilizing an observer that can incorporate the effect the fins have in a VCC system could also contribute to improved performance significantly. Therefore, the overall purpose of this thesis was to:

1. Identify effective heat transfer coefficients for each heat exchanger.
    a. Use these coefficients to calibrate a controls-oriented lumped parameter model to published system performance.
2. Develop a nonlinear state observer that utilizes this new lumped parameter model that can be used to monitor a physical system.

Goal number 1 was accomplished as shown in chapter three, where overall heat transfer coefficients were defined that could incorporate the impact of the fin geometry into a controls-oriented system. Using data provided by the manufacturer, functions were defined in chapter four for these coefficients that calibrated the lumped parameter model to the published data. The modified dynamic model (utilizing these coefficients) was able

to predict the heat removed by the VCC within only ±4% error when compared to the published system performance.

Goal number 2 was accomplished as shown in chapter 5, where a variety of observers were tested for their feasibility of use in estimating the states of the system while utilizing the new lumped parameter model (which incorporates the effective fin coefficients). It was concluded that a 4-measurement observer would be the best place to start when testing this model with a physical system as it had the fastest convergence time. It was also determined that at least one pressure measurement is necessary to develop a stable nonlinear state observer for this system.

Future Work

While the results outlined throughout this thesis are very promising, they still need to be verified experimentally. As previously mentioned, it would be recommended to start by testing the four-measurement nonlinear observer on the actual physical system. Furthermore, a more extensive calibration of the effective heat transfer coefficients could be obtained by testing the system over an even greater range of conditions (as compared to those provided by the manufacturer). For example, the effective heat transfer coefficient for the evaporator proved to be dependent on both the wet and dry bulb temperatures of the air surrounding the heat exchanger. Therefore, the effective heat transfer coefficient for the condenser could likely be improved by refining the calibration with more detail about the surrounding environment (such as; humidity, elevation, etc.), than that provided by the manufacturer.

The dynamic model proved to be very sensitive to the limitations of the CoolProp library, specifically its ability to predict properties within the saturated region for non-

pure substances like the R410a used within the Goodman unit studied. Because of this, adapting this model to another system might provide insight into improving the ability to withstand a greater range of heat transfer mediums used throughout industry.

REFERENCES

Bell, I. H., Wronski, J., Quoilin, S., & Lemort, V. (2014). Pure and Pseudo-pure Fluid Thermophysical Property Evaluation and the Open-Source Thermophysical Property Library CoolProp. *Industrial & Engineering Chemistry Research, 53*(6), 2498-2508.

Cengel, Y., & Boles, M. (2015). *Thermodynamics An Engineering Approach.* New York: McGraw Hill.

Cheng, T. (2002). *Nonlinear Observer Design Using Contraction Theory with Application to Heat Exchangers Having Varying Phase Transition.* Massachusetts Institute of Technology.

Cheng, T., Asada, H. H., He, X.-D., & Kasahara, S. (2005). Heat Exchanger Dynamic Observer Design. *ASHRAE Transactions, Volume 111 Issue 1*, 328-335.

Frink, B. S. (2005). *Modeling and Construction of a Computer Controlled Air Conditioning System.* Manhattan: Kansas State University.

Gardner, J., & Luthman, H. (2016). Paramater Estimation for HVAC System Models from Standard Test Data.

Goodman Air Conditioning & Heating. (n.d.). *Goodman GSX13 Manual.* Retrieved January 2017, from https://www.manualslib.com/manual/1124934/Goodman-Gsx13.html

He, X.-D. (1996). *Dynamic Modeling and Multivariable Control of Vapor Compression Cycles in Air Conditioning Systems.*

Kulakowski, B. T., Gardner, J. F., & Shearer, L. J. (2007). *Dynamic Modeling and Control of Engineering Systems.* New York: Cambridge University Press.

Li, B. (2009). *A Dynamic Model of a Vapor Compression Cycle with Shut-Down and Start-Up Operations.*

Lohmiller, W., & Slotine, J.-J. E. (1998). On Contraction Analysis for Non-linear Systems. *Automatica, Vol. 34, No. 5,* 683-696.

Luthman, H. (2016). *Paramater Estimation for HVAC System Models from Standard Test Data.*

Matko, D., Geiger, G., & Werner, T. (2001). Modelling of the Pipeline as a Lumped Parameter System. *Automatika, 42,* 177-188.

McKinley, T. L., & Alleyne, A. G. (2008). An advanced nonlinear switched heat exchanger model for vapor compression cycles using the moving-boundary method. *Internation Journal of Refrigeration, 31,* 1253 - 1264.

Oppenheim, A. V., & Verghese, G. C. (2010). *6.011 Introduction to Communication, Control, and Signal Processing Spring 2010.* Retrieved from Massachusetts Institute of Technology: MIT OpenCourseWare: https://ocw.mit.edu/

Rasmussen, B. P. (2005). *Dynamic Modeling and Advanced Control of Air Conditioning and Refrigeration Systems.* Urbana: University of Illinois.

Smith, M. K., Wattelet, J. P., & Newell, T. A. (1993). *A Study of Evaporation Heat Transfer Coefficient Correlations at Low Heat and Mass Fluxes for Pure Refrigerants and Refrigerant Mixtures.* Urbana: Air Conditioning and Refrigeration Center University of Illinois.

APPENDIX A

Example Manufacturer Data Set

Figure 22, below shows a sample of the data on air conditioner performance for different conditions available from the manufacturer. (Goodman Air Conditioning & Heating)

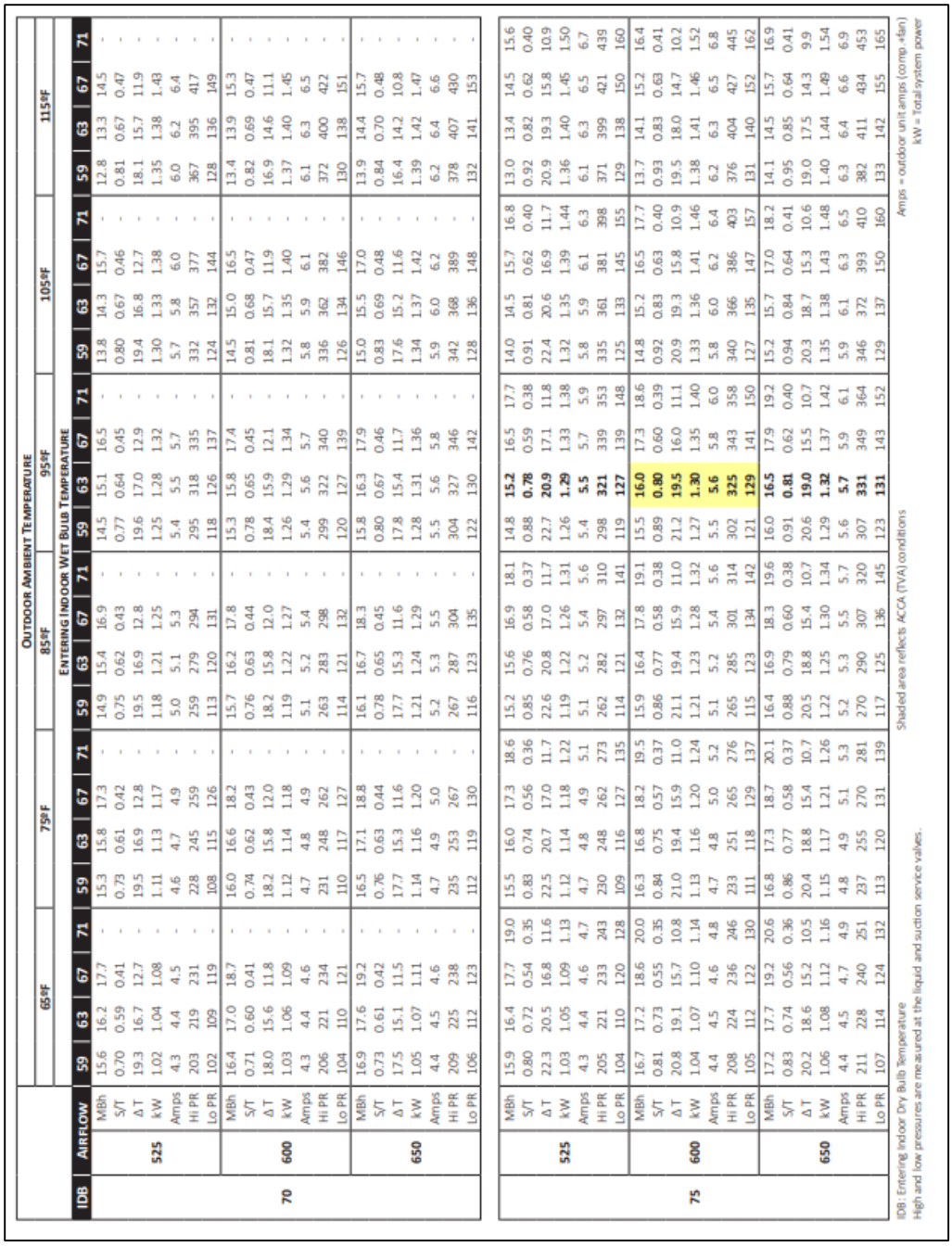

IDB	Airflow		Outdoor Ambient Temperature 65°F Entering Indoor Wet Bulb Temperature 59	63	67	71	75°F 59	63	67	71	85°F 59	63	67	71	95°F 59	63	67	71	105°F 59	63	67	71	115°F 59	63	67	71
70	525	MBh	15.6	16.2	17.7	-	15.3	15.8	17.3	-	14.9	15.4	16.9	-	14.5	15.1	16.5	-	13.8	14.3	15.7	-	12.8	13.3	14.5	-
		S/T	0.70	0.59	0.41	-	0.73	0.61	0.42	-	0.75	0.62	0.43	-	0.77	0.64	0.45	-	0.80	0.67	0.46	-	0.81	0.67	0.47	-
		ΔT	19.3	16.7	12.7	-	19.5	16.9	12.8	-	19.5	16.9	12.8	-	19.6	17.0	12.9	-	19.4	16.8	12.7	-	18.1	15.7	11.9	-
		kW	1.02	1.04	1.08	-	1.11	1.13	1.17	-	1.18	1.21	1.25	-	1.25	1.28	1.32	-	1.30	1.33	1.38	-	1.35	1.38	1.43	-
		Amps	4.3	4.4	4.5	-	4.6	4.7	4.9	-	5.0	5.1	5.3	-	5.4	5.5	5.7	-	5.7	5.8	6.0	-	6.0	6.2	6.4	-
		Hi PR	203	219	231	-	228	245	259	-	259	279	294	-	295	318	335	-	332	357	377	-	367	395	417	-
		Lo PR	102	109	119	-	108	115	126	-	113	120	131	-	118	126	137	-	124	132	144	-	128	136	149	-
	600	MBh	16.4	17.0	18.7	-	16.0	16.6	18.2	-	15.7	16.2	17.8	-	15.3	15.8	17.4	-	14.5	15.0	16.5	-	13.4	13.9	15.3	-
		S/T	0.71	0.60	0.41	-	0.74	0.62	0.43	-	0.76	0.63	0.44	-	0.78	0.65	0.45	-	0.81	0.68	0.47	-	0.82	0.69	0.47	-
		ΔT	18.0	15.6	11.8	-	18.2	15.8	12.0	-	18.2	15.8	12.0	-	18.4	15.9	12.1	-	18.1	15.7	11.9	-	16.9	14.6	11.1	-
		kW	1.03	1.06	1.09	-	1.12	1.14	1.18	-	1.19	1.22	1.27	-	1.26	1.29	1.34	-	1.32	1.35	1.40	-	1.37	1.40	1.45	-
		Amps	4.3	4.4	4.6	-	4.7	4.8	4.9	-	5.1	5.2	5.4	-	5.4	5.6	5.7	-	5.8	5.9	6.1	-	6.1	6.3	6.5	-
		Hi PR	206	221	234	-	231	248	262	-	263	283	298	-	299	322	340	-	336	362	382	-	372	400	422	-
		Lo PR	104	110	121	-	110	117	127	-	114	121	132	-	120	127	139	-	126	134	146	-	130	138	151	-
	650	MBh	16.9	17.6	19.2	-	16.5	17.1	18.8	-	16.1	16.7	18.3	-	15.8	16.3	17.9	-	15.0	15.5	17.0	-	13.9	14.4	15.7	-
		S/T	0.73	0.61	0.42	-	0.76	0.63	0.44	-	0.78	0.65	0.45	-	0.80	0.67	0.46	-	0.83	0.69	0.48	-	0.84	0.70	0.48	-
		ΔT	17.5	15.1	11.5	-	17.7	15.3	11.6	-	17.7	15.3	11.6	-	17.8	15.4	11.7	-	17.6	15.2	11.6	-	16.4	14.2	10.8	-
		kW	1.05	1.07	1.11	-	1.14	1.16	1.20	-	1.21	1.24	1.29	-	1.28	1.31	1.36	-	1.34	1.37	1.42	-	1.39	1.42	1.47	-
		Amps	4.4	4.5	4.6	-	4.7	4.9	5.0	-	5.2	5.3	5.5	-	5.5	5.6	5.8	-	5.9	6.0	6.2	-	6.2	6.4	6.6	-
		Hi PR	209	225	238	-	235	253	267	-	267	287	304	-	304	327	346	-	342	368	389	-	378	407	430	-
		Lo PR	106	112	123	-	112	119	130	-	116	123	135	-	122	130	142	-	128	136	148	-	132	141	153	-
75	525	MBh	15.9	16.4	17.7	19.0	15.5	16.0	17.3	18.6	15.2	15.6	16.9	18.1	14.8	**15.2**	16.5	17.7	14.0	14.5	15.7	16.8	13.0	13.4	14.5	15.6
		S/T	0.80	0.72	0.54	0.35	0.83	0.74	0.56	0.36	0.85	0.76	0.58	0.37	0.88	**0.78**	0.59	0.38	0.91	0.81	0.62	0.40	0.92	0.82	0.62	0.40
		ΔT	22.3	20.5	16.8	11.6	22.5	20.7	17.0	11.7	22.6	20.8	17.0	11.7	22.7	**20.9**	17.1	11.8	22.4	20.6	16.9	11.7	20.9	19.3	15.8	10.9
		kW	1.03	1.05	1.09	1.13	1.12	1.14	1.18	1.22	1.19	1.22	1.26	1.31	1.26	**1.29**	1.33	1.38	1.32	1.35	1.39	1.44	1.36	1.40	1.45	1.50
		Amps	4.3	4.4	4.6	4.7	4.7	4.8	4.9	5.1	5.1	5.2	5.4	5.6	5.4	**5.5**	5.7	5.9	5.8	5.9	6.1	6.3	6.1	6.3	6.5	6.7
		Hi PR	205	221	233	243	230	248	262	273	262	282	297	310	298	**321**	339	353	335	361	381	398	371	399	421	439
		Lo PR	104	110	120	128	109	116	127	135	114	121	132	141	119	**127**	139	148	125	133	145	155	129	138	150	160
	600	MBh	16.7	17.2	18.6	20.0	16.3	16.8	18.2	19.5	15.9	16.4	17.8	19.1	15.5	**16.0**	17.3	18.6	14.8	15.2	16.5	17.7	13.7	14.1	15.2	16.4
		S/T	0.81	0.73	0.55	0.35	0.84	0.75	0.57	0.37	0.86	0.77	0.58	0.38	0.89	**0.80**	0.60	0.39	0.92	0.83	0.63	0.40	0.93	0.83	0.63	0.41
		ΔT	20.8	19.1	15.7	10.8	21.0	19.4	15.9	11.0	21.1	19.4	15.9	11.0	21.2	**19.5**	16.0	11.1	20.9	19.3	15.8	10.9	19.5	18.0	14.7	10.2
		kW	1.04	1.07	1.10	1.14	1.13	1.16	1.20	1.24	1.21	1.23	1.28	1.32	1.27	**1.30**	1.35	1.40	1.33	1.36	1.41	1.46	1.38	1.41	1.46	1.52
		Amps	4.4	4.5	4.6	4.8	4.7	4.8	5.0	5.2	5.1	5.2	5.4	5.6	5.5	**5.6**	5.8	6.0	5.8	6.0	6.2	6.4	6.2	6.3	6.5	6.8
		Hi PR	208	224	236	246	233	251	265	276	265	285	301	314	302	**325**	343	358	340	366	386	403	376	404	427	445
		Lo PR	105	112	122	130	111	118	129	137	115	123	134	142	121	**129**	141	150	127	135	147	157	131	140	152	162
	650	MBh	17.2	17.7	19.2	20.6	16.8	17.3	18.7	20.1	16.4	16.9	18.3	19.6	16.0	**16.5**	17.9	19.2	15.2	15.7	17.0	18.2	14.1	14.5	15.7	16.9
		S/T	0.83	0.74	0.56	0.36	0.86	0.77	0.58	0.37	0.88	0.79	0.60	0.38	0.91	**0.81**	0.62	0.40	0.94	0.84	0.64	0.41	0.95	0.85	0.64	0.41
		ΔT	20.2	18.6	15.2	10.5	20.4	18.8	15.4	10.7	20.5	18.8	15.4	10.7	20.6	**19.0**	15.5	10.7	20.3	18.7	15.3	10.6	19.0	17.5	14.3	9.9
		kW	1.06	1.08	1.12	1.16	1.15	1.17	1.21	1.26	1.22	1.25	1.30	1.34	1.29	**1.32**	1.37	1.42	1.35	1.38	1.43	1.48	1.40	1.44	1.49	1.54
		Amps	4.4	4.5	4.7	4.9	4.8	4.9	5.1	5.3	5.2	5.3	5.5	5.7	5.6	**5.7**	5.9	6.1	5.9	6.1	6.3	6.5	6.3	6.4	6.6	6.9
		Hi PR	211	228	240	251	237	255	270	281	270	290	307	320	307	**331**	349	364	346	372	393	410	382	411	434	453
		Lo PR	107	114	124	132	113	120	131	139	117	125	136	145	123	**131**	143	152	129	137	150	160	133	142	155	165

IDB : Entering Indoor Dry Bulb Temperature
High and low pressures are measured at the liquid and suction service valves.
Shaded area reflects ACCA (TVA) conditions
Amps = outdoor unit amps (comp +fan)
kW = Total system power

Figure 22. Sample Manufacturer's Performance Data.

APPENDIX B

Compressor Model

The compressor model used throughout this thesis was provided by the manufacturer, Emerson (via personal communication, March 2017), as it directly corresponds to the compressor utilized within the Goodman AC unit studied.

$$\dot{m} = f(T_c, T_e) \tag{35}$$

Where:

$\dot{m}$ – is the mass flowrate out of the compressor [lbm/hr]

T_c – is the condensing temperature within the condenser [°F]

P_e – is the pressure through the evaporator [°F]

$$\dot{m} = M_0 + (M_1 T_e) + (M_2 T_c) + \left(M_3 {T_e}^2\right) + (M_4 T_e T_c) + \left(M_5 {T_c}^2\right) + \left(M_6 {T_e}^3\right) + \left(M_7 T_c {T_e}^2\right) + \left(M_8 T_e {T_c}^2\right) + \left(M_9 {T_c}^3\right) \tag{36}$$

Table 8 below shows the values for each coefficient found in Equation (36).

Table 8. Emerson Compressor Coefficients

Coefficient	Value
M_0	175.112137644863
M_1	2.80638926148068
M_2	-1.40787558254641
M_3	0.026420018352226
M_4	0.000140311440855487
M_5	0.0136958997870442
M_6	0.0000655313316488453
M_7	2.79416989914196E-06
M_8	-2.73216081223254E-6
M_9	-0.0000533435773331436

APPENDIX C

Four-Measurement Observer Convergence Plots

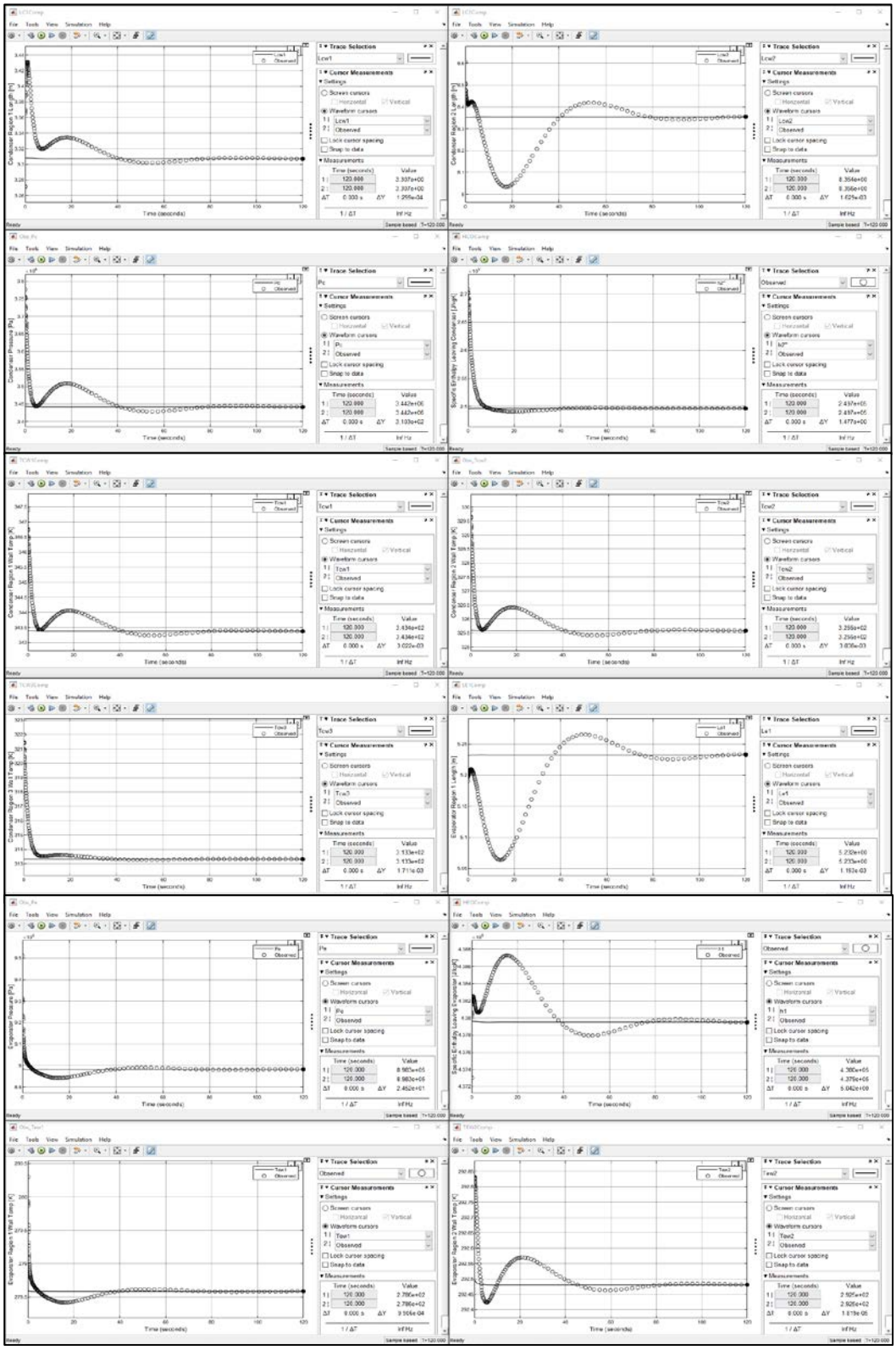

Figure 23. Convergence plots for measured and estimated states of the 4-measurement observer.